Synthesis and Optical Properties of Strontium Hexaferrite ($SrFe_{12}O_{19}$) Fibers by Electrospinning

Ronariddh Nakhowong [a, b,*], Sert Kiennork [a], Pakawat Wongwanwattana [a], Romteera Chueachot [b, c]

[a] *Program of Physics, Faculty of Science, Ubon Ratchathani Rajabhat University, Ubon Ratchathani, 34000 Thailand*
[b] *Functional Nanomaterials and Electrospinning Research Laboratory, Faculty of Science, Ubon Ratchathani Rajabhat University, Ubon Ratchathani, 34000 Thailand*
[c] *Program of Chemistry, Faculty of Science, Ubon Ratchathani Rajabhat University, Ubon Ratchathani, 34000 Thailand*

Received 15 August 2018; Revised 11 September 2018; Accepted 11 September 2018

Abstract

The strontium hexaferrite fibers ($SrFe_{12}O_{19}$) were synthesized by electrospinning using iron (III) nitrate, strontium nitrate and polyacrylonitrile (PAN) as precursors. The as-spun fibers were calcined at 900, 1000 and 1100 ºC for 8 h in air. The as-spun and calcined fibers were characterized by thermogravimetric-differential thermal analysis (TG-DTA), X-ray diffraction (XRD), Field emission scanning electron microscopy (FE-SEM), Fourier transform infrared spectroscopy (FT-IR) and UV-Visible diffuse reflectance spectroscopy (UV-Vis DRS). The TG-DTA results showed that completely decomposition of PAN and formation of the crystallization occurred above 500 ºC. The XRD and FT-IR results confirmed the crystalline phases of $SrFe_{12}O_{19}$ and impurity phase of -Fe_2O_3 were detected. FE-SEM images showed that the $SrFe_{12}O_{19}$ fibers had porosity and rough surface with diameter about 500 – 1200 nm. UV-Vis DRS spectra showed that $SrFe_{12}O_{19}$ fibers exhibit the absorption bands in range of ultraviolet and visible light regions. The band gap energy of $SrFe_{12}O_{19}$ fibers is about 2.00 eV in different temperatures.

KEYWORDS: GVL; Strontium hexaferrite; Optical properties; Fiber technology; Electrospinning

* Corresponding authors; e-mail: ronariddh.n@ubru.ac.th

Introduction

The M-type nanohexaferites (M = Pb, Sr and Ba) plays an important role in hare magnetic materials. The M-hexaferrites have much attention due to their high coercivity, magnetization, and magnetocrystalline anisotropy, which can be used as permanent magnets [1]. The M-hexaferrites are more used in high density recordings media, permanent magnets, data storage devices and microwave frequency in electrical devices [1]. The strontium hexaferrite ($SrFe_{12}O_{19}$) with hexagonal magnetoplumbite structure is typical hard magnetic material with a high saturation magnetization, coercivity, Curie temperature and magnetocrystalline anisotropy [2]. The $SrFe_{12}O_{19}$ is attractive due to its good chemical stability, mechanical hardness, low cost, low density, large electrical resistivity and high microwave magnetic losses [3]. The $SrFe_{12}O_{19}$ has been synthesized in various methods including citrate sol-gel combustion approach [1], sol-gel routh [4], solid phase method [5], co-precipitation method [6], hydrothermal process [7], ceramic route [8], and electrospinning [2]. One dimensional (1D) nanostructures have the advantages of high aspect ratio, high interfacial area, and shortest pathway for ion diffusion, compared with other nanostructures [9]. The electrospinning is a new, simple, versatile and cost-effective method for fabricating ultrafine fibers with diameters ranging from tens of nanometers to submicrometer [10]. With the high surface area, tunable porosity, electrospun fibers have been applied in several fields, such as tissue engineering, biosensors, filtration, wound dressings, drug delivery, enzyme immobilization and electronic devices [11]. In the paper, we report the strontium hexaferrite fibers prepared by combination of electrospinning and calcination processes.

The thermal stability, crystalline phase, morphology, functional groups, and optical properties were investigated.

Materials and Methods

The strontium hexaferrite ($SrFe_{12}O_{19}$) fibers were synthesized by electrospinning and calcination processes. In a typical procedure, strontium nitrate ($Sr(NO_3)_2$, Acros Organics) and Iron(III) nitrate nonahydrate ($Fe(NO_3)_3 \cdot 9H_2O$, Carlo Erba reagents) in a molar ratio corresponding to the nominal composition of $SrFe_{12}O_{19}$ were dissolved in 10 mL of *N*,*N*-Dimethylformamide (DMF, $HCON(CH_3)_2$, Acros Erba) and magnetic stirring for 1 h to get a clear solution. Then, 0.65 g of polyacrylonitrile (PAN, M_w = 150000 Sigma Aldrich) were added to above solution with continuous stirring for 12 to obtain mixed solution. The mixed solution was loaded into a plastic syringe with a stainless steel needle. A voltage of 17 kV was applied between the needle tip and collector. The tip and collector were fixed at 15 cm. The as-spun fibers were calcined at 900, 1000 and 1100 ºC for 8 h in air. The thermal property of the as-spun fibers was recorded by thermogravimetric and differential thermal analysis (TG-DTA, Thermo plus TG8120, Rigaku, Japan). The crystalline phases were performed by by X-ray diffraction (XRD, Phillips, X pert' MPD, Netherlands) using Cu*K*α radiation with λ = 0.15418 nm. The morphology of fibers was observed by Field emission scanning electron microscopy (FE-SEM, JSM 6335 F, Japan). UV-Vis diffuse reflectance spectra (UV-Vis DRS) were recorded using UV-Vis spectrophotometer (T90+, PG Instruments, United kingdom) attached to an integrating sphere with $BaSO_4$ as a reference. The functional groups of the samples were carried out by Fourier transform infrared spectroscopy (FT-IR, Bruker, Tensor II, Germany).

Results and Discussion

Fig. 1 shows TG-DTA curves of the as-spun fibers. The TGA curve exhibits three steps of weight loss processes. The first minor step of weight loss (~18%) below 173 ºC is ascribed to the evaporation of the absorbed water and trapped solvent in the as-spun fibers [12]. The second step of weight loss (~50%) at 174 – 350 ºC was due to the decomposition of nitrile groups, and the cyclization of the nitrile groups of PAN [12 – 13]. The third step of weight loss at 351 – 500 ºC corresponded to completely decomposition of the PAN main chain, which was in agreement with DTA curve. The strong exothermic peaks at 318 and 479 ºC were attributed to the cyclization of the nitrile groups of PAN and the transformation of the amorphous phase to crystalline phase [13]. The broad exothermic peaks at 601 and 800 ºC were attributed the formation of the metal oxide and the oxidation of carbon, carbon monoxide, respectively [13]. No further significant weight loss is observed above 500 ºC, indicating that the completely decomposition of PAN and organic compounds resulting the formation of $SrFe_{12}O_{19}$ fibers.

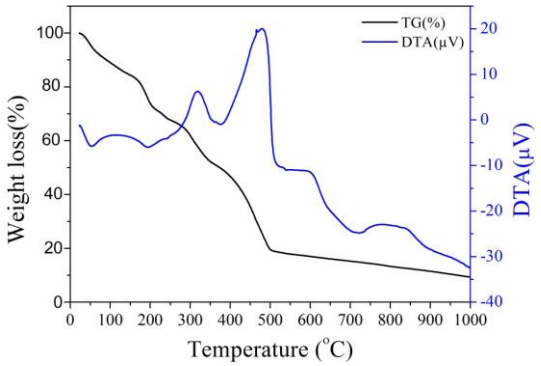

Fig. 1 TG-DTA curves of as-spun fibers.

Fig. 2 shows the XRD patterns of $SrFe_{12}O_{19}$ fibers calcined at 900 – 1100 ºC for 8 h in the air. The XRD pattern of the as-spun fibers (Fig. 2a) showed that no diffraction patterns were observed due to amorphous nature of the polymer. The peak at 2θ = 17° corresponding to the orthorhombic PAN (110) reflection were detected [14]. At the calcination temperature of 900 ºC (Fig. 2b), characteristic diffraction patterns are in good agreement with hexagonal structure of $SrFe_{12}O_{19}$ phases (JCPDS Card 33-1340, space group P63/mmc (194)) and impurity phase of α -Fe_2O_3 (JCPDS Card 33-0064) were detected [5]. The impurity phase of α -Fe_2O_3 is due to the loss of Sr ions in the thermal decomposition process, which caused the surplus Fe ions changed to Fe_2O_3 eventually [15]. After increasing calcination at 1000 and 1100 ºC (Figs. 4 c and d), the diffraction peaks became sharper with higher intensity, indicating increased crystallinity of $SrFe_{12}O_{19}$.

Fig. 3 shows FT-IR spectra of the as-spun fibers and $SrFe_{12}O_{19}$ fibers at different temperatures. It can be seen that the absorption bands of the as-spun fibers in ranging from 1000 to 2500 cm^{-1} are attributed to stretching and bending vibration of PAN [13]. The peak at 2243 cm^{-1} is assigned to the stretching vibration of nitrile groups ($C \equiv N$) in PAN chain [16]. The peak at 1451 cm^{-1} is assigned to symmetrical

bending vibration of methylene groups [16]. The peaks at 1334 and 3426 cm^{-1} are attributed to NO_3^- and –OH stretching vibration [13]. It was seen that the absorption bands of PAN disappeared due to decomposition of PAN at high temperature. After the calcination at 900, 1000 and 1100 ºC, the peaks at 435, 561, and 608 cm^{-1} are assigned to stretching vibrations of $SrFe_{12}O_{19}$ [17].

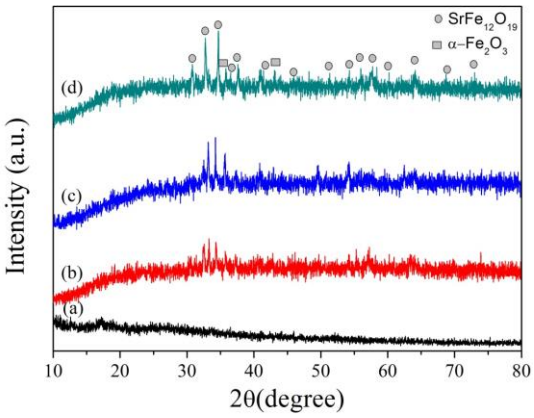

Fig. 2 XRD patterns of $SrFe_{12}O_{19}$ fibers: (a) as-spun fibers, (b) fibers calcined at 900 ºC, (c) fibers calcined at 1000 ºC and (d) fibers calcined at 1100 ºC.

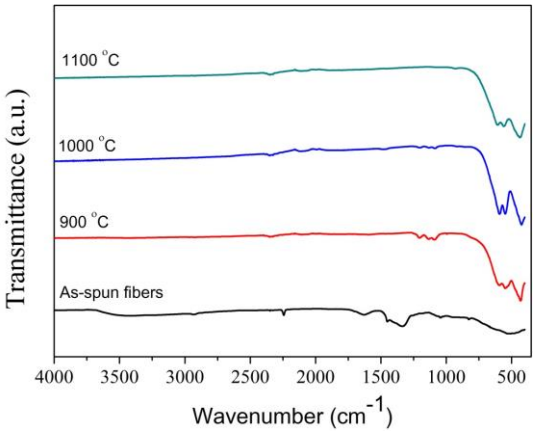

Fig. 3 FT-IR spectra of the as-spun fibers and $SrFe_{12}O_{19}$ fibers at different temperatures.

The surface morphology of the as-spun and $SrFe_{12}O_{19}$ fibers are shown in Fig. 4. The as-spun fibers (Fig. 4a) appear to be smooth surface without any bead due to the amorphous nature of the polymer. The average diameter of the as-spun fibers is about 885 nm. After the as-spun fibers calcined at 900 ºC, it observed that the fibers became rougher and porous due to calcination because of the decomposition of PAN and the crystallization of inorganic phases as shown in Fig. 4b. The fiber diameter decreased to 580 nm due to burn out of PAN and formation of $SrFe_{12}O_{19}$ fibers. When increase calcination to 1000 ºC, the fiber appear the shrinkage with diameter about 526 nm. Moreover, it revealed that $SrFe_{12}O_{19}$ fibers were made up of several particles connected together to formation of the fibers. Further increasing the calcination temperature to 1100 ºC (Fig. 4d), the fibers were transformed to curled surface like largely linked poly crystalline particles with an average diameter of 785 nm. The increasing of the fiber diameter is due to increasing of the grain sizes and the improvement of the crystallizations.

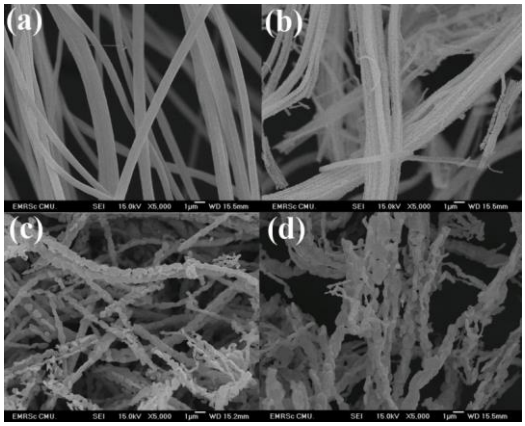

Fig. 4 FE-SEM images of $SrFe_{12}O_{19}$ fibers: (a) the as-spun fibers, (b) fibers calcined at 900, (c) 1000 and (d) 1100 ºC.

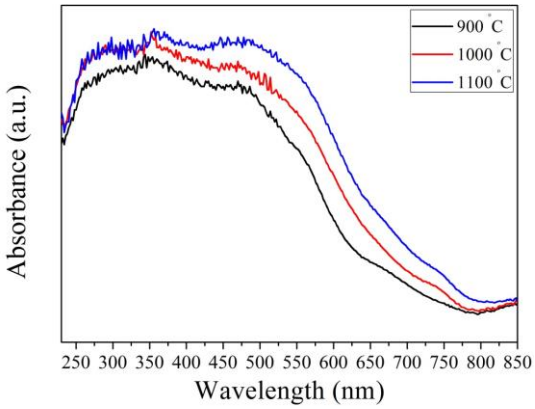

Fig. 5 UV-Vis DRS spectra of $SrFe_{12}O_{19}$ fibers calcined at different temperatures.

The UV-Vis DRS spectra of $SrFe_{12}O_{19}$ fibers are shown in Fig.5. The absorption spectra of $SrFe_{12}O_{19}$ fibers revealed that the absorption bands are in range of visible light and strong absorption in UV light region. It was observed

that the intensity of absorption peaks of $SrFe_{12}O_{19}$ fibers were increased with increasing calcination temperature.

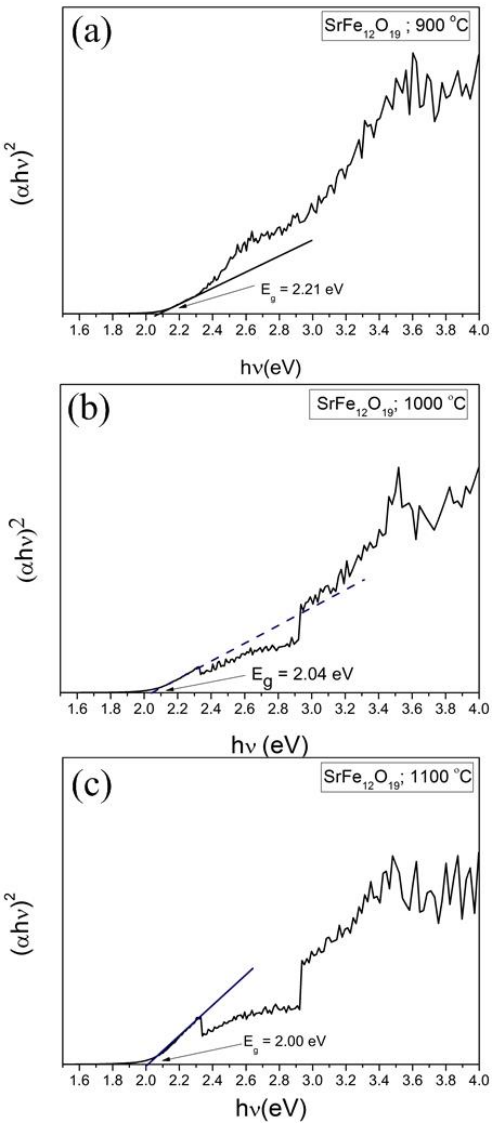

Fig. 6 Band gap energy of $SrFe_{12}O_{19}$ fibers calcined at (a) 900, (b) 1000 and (c) 1100 ºC.

The band gap energy (E_g) of $SrFe_{12}O_{19}$ fibers at different temperatures are shown in Fig. 6. A Tauc plot was evaluated the band gap energy of $SrFe_{12}O_{19}$ fibers is shown in Fig. 6. The band gap energy was calculated from the relation [18, 19]:

$$[F(R)h\nu]^2 = A(h\nu - E_g) \quad (1)$$

where $h\nu$, A and $F(R)$ denote the photon energy, the proportionality constant and Kubelka-Munk function, respectively. The Kubelka-Munk function was evaluated following formula [18, 20]:

$$F(R) = \frac{(1-R)^2}{2R} \quad (2)$$

where R is the absorption value.

The E_g was estimated by plotting $[F(R)h\nu]^2$ versus $h\nu$ by extrapolating the tangent line of the curve to zero. The values of E_g were 2.09, 2.04 and 2.00 eV calcined at 900, 1000 and 1100 ºC, respectively. Mishra et al. [21] reported that $SrFe_{12}O_{19}$ powders exhibit the direct (E_d) and indirect band gap energies (E_{ind}) of 1.70 eV and 0.83 eV, respectively. The band gap energy showed tendency increase due to the different of crystallite size, particle size, porosity and preparation method.

Conclusion

In summary, $SrFe_{12}O_{19}$ fibers were successfully synthesized by combined electrospinning and calcination processes. XRD and FT-IR results showed that crystalline phases $SrFe_{12}O_{19}$ were obtained at high temperature. SEM images revealed the 1D nanostructure with porosity and shrinkage due to decomposition of PAN and formation of $SrFe_{12}O_{19}$ fibers. The optical properties showed that calcined fibers exhibits the absorption bands in visible light and strong absorption in UV light regions. The band gap energies of the samples were decreased with the increasing calcination temperature. The electrospinning might open a new route for the fibrous technology and applications in electronic devices.

Acknowledgements

The authors are grateful for the support and funding from Ubon Ratchathani Rajabhat University, Thailand.

References

[1] M.A. Almessiere, Y. Slimani, H. Güngüneş, H.S. El Sayed, A. Baykal, AC susceptibility and Mossbauer study of Ce^{3+} ion substituted $SrFe_{12}O_{19}$ nanohexaferrites, Ceram. Int. 44 (2018) 10470 – 10477.

[2] Q. Liang, X. Shen, F. Song, M. Liu, Fabrication and magnetic property of one-dimensional $SrTiO_3/SrFe_{12}O_{19}$ composite nanofibers by electrospinning, J. Mater. Sci. Technol. 27 (2011) 996 – 1000.

[3] T. Zhang, X. Peng, J. Li, Y. Yang, J. Xu, P. Wang, D. Jin, H. Jin, B. Hong, X. Wang, H. Ge, Structural, magnetic and electromagnetic properties of $SrFe_{12}O_{19}$ ferrite with particles aligned in a magnetic field, J. Alloys Compd. 690(2017) 936 – 941.

[4] T. Li, Y. Li, R. Wu, H. Zhou, X. Fang, S. Su, A. Xia, C. Jin, X. Liu, A solution for the preparation of hexagonal M-type $SrFe_{12}O_{19}$ ferrite using egg-white: Structural and magnetic properties, J. Magn. Magn. Mater. 393 (2015) 325 – 330.

[5] P. Long, L. Lezhong, W. Rui, T. Xiaoqiang, H. Yun, H. Yuebin, G. Cheng, Characteristics improvement of low-temperature sintered $SrFe_{12}O_{19}$ ferrites in LTCC system applications, Rare Metal Mat Eng. 45 (2016) 3095 – 3098.

[6] V. Harikrishnan, P. Saravanan, R.E. Vizhi, D.R. Babu, V.T.P. Vinod, P. Kejzlar, M. Černík, Effect of annealing temperature on the structural and magnetic properties of CTAB-capped $SrFe_{12}O_{19}$ platelets, J. Magn. Magn. Mater. 401 (2016) 775 – 783.

[7] C. Zhao, M. Shen, Z. Li, R. Sun, A. Xia, X. Liu, Green synthesis and enhanced microwave absorption property of reduced graphene oxide- $SrFe_{12}O_{19}$ nanocomposites, J. Alloys Compd. 689 (2016) 1037 – 1043.

[8] R. Sun, X. Li, A. Xia, S. Su, C. Jin, Hexagonal $SrFe_{12}O_{19}$ ferrite with high saturation magnetization, Ceram. Int. 44 (2018) 13551 – 13555.

[9] S. Vijayakumar, S.H. Lee, K.S. Ryu, Hierarchical $CuCo_2O_4$ nanobelts as a supercapacitor electrode with high areal and specific capacitance, Electrochimic. Acta, 182 (2015) 979 – 986.

[10] Z.M. Huang, Y.Z. Zhang, M. Kotaki, S. Ramakrishna, A review on polymer nanofibers by electrospinning and their applications in nanocomposites, Compos. Sci. Technol. 63 (2003) 2223 – 2253.

[11] N. Bhardwaj, S.C. Kundu, Electrospinning: A fascinating fiber fabrication technique, Biotechnol. Adv. 28 (2010) 325 – 347.

[12] H. Yu, J. Guo, S. Zhu, Y. Li, Q. Zhang, M. Zhu, Preparation of continuous alumina nanofibers via electrospinning of PAN/DMF solution, Mater. Lett. 74(2012) 247 – 249.

[13] R. Nakhowong, R. Chueachot, Synthesis and magnetic properties of copper cobaltite ($CuCo_2O_4$) fibers by electrospinning, J. Alloys Compd. 715 (2017) 390 – 396.

[14] C. Peng J. Zhang, Z. Xiong, B. Zhao, P. Liu, Fabrication of porous hollow γ-Al_2O_3 nanofibers by facile electrospinning and its application for water remediation, Microporous Mesoporous Mater. 215 (2015) 133 – 142.

[15] Q. Wu, Z. Yu, Y. Wu, Z. Gao, H. Xie, The magnetic and photocatalytic properties of nanocomposites $SrFe_{12}O_{19}/ZnFe_2O_4$, J. Magn. Magn. Mater. 465 (2018) 1 – 8.

[16] P. Liu, Y. Zhu, J. Ma, S. Yang, J. Gong, J. Xu, Preparation of continuous porous alumina nanofibers with hollow structure by single capillary electrospinning, Colloids Surf. A. 436 (2013) 489 – 494.

[17] T. Li, Y. Li, R. Wu, H. Zhou, X. Fang, S. Su, A. Xia, C. Jin, X. Liu, A solution for the preparation of hexagonal M-type $SrFe_{12}O_{19}$ ferrite using egg-white: Structural and magnetic properties. J. Magn. Magn. Mater. 393 (2015) 325 – 330.

[18] R. Nakhowong, S. Kiennork, P. Wongwanwattana, T. Seetawan, R. Chueachot, Synthesis, structural and optical properties of electrospun magnesium aluminate nanofibers, Mater. Lett. 220 (2018) 234 – 237.

[19] D.D. Mishra, G. Tan, Visible photocatalytic degradation of methylene blue on magnetic $SrFe_{12}O_{19}$, J. Phys. Chem. Solids 123 (2018) 157 – 161.

[20] G.C. Leindecker, A.K. Alves, C.P. Bergmann, Synthesis of niobium oxide fibers by electrospinning and characterization of their morphology and optical properties, Ceram. Int. 40 (2014) 16195 – 16200.